

## Packing a flexible fiber into a cavity

J. D. Sherwood 

*Department of Applied Mathematics and Theoretical Physics, University of Cambridge, Cambridge CB3 0WA, United Kingdom*

S. Ghosal 

*Department of Mechanical Engineering and Engineering Sciences and Applied Mathematics,  
Northwestern University, Evanston, Illinois 60208, USA*



(Received 2 January 2022; accepted 7 March 2022; published 25 March 2022)

The insertion of an elastic rod or fiber into a confining cavity is studied. Such an insertion is a feature of a variety of problems, including packing and unpacking of DNA in viral capsids and the insertion of catheters during surgery. We consider a simplified geometry in which the container is a smooth (frictionless) circular cylinder of radius  $a$ . The fiber is pushed through a hole in the curved surface of the cylinder and is then assumed to stay in a cross-sectional plane perpendicular to the cylinder axis. A solution is found for the fiber shape in which most of the fiber lies against the curved interior surface of the cylinder, apart from the final end section of the fiber, of length  $2.0888a$ , which crosses the interior of the cylinder before ending at the opposite side, which it meets at an angle  $1.15$  rad to the normal. The force required to push the fiber into the cylinder is  $EI/2a^2$ , where  $E$  is the fiber's Young's modulus and  $I$  its cross-sectional moment of inertia. The shape of the final end section of the fiber is confirmed by experiment.

DOI: [10.1103/PhysRevE.105.035002](https://doi.org/10.1103/PhysRevE.105.035002)

### I. INTRODUCTION

The interaction between an elastic fiber and confining walls plays an important role in a variety of problems on macro- as well as micro- and nanoscales. A classic example of the latter is the packing and unpacking of DNA into viral cavities in various phases of the life cycle of certain viruses known as “bacteriophages.” The genetic material of the phage is enclosed in a protein capsid that encloses and protects it [1]. During infection, the DNA alone is injected into the cell while the capsid remains attached to the cell membrane. In certain cases, the release of elastic and electrostatic energy of the stiff DNA polymer confined within the viral capsid [2] is the driving force responsible for the ejection [3]. Experiments and numerical simulations have confirmed that DNA within viral capsids [4–7] packs in much the same way as wires and fibers in large-scale mechanical models [8–15]. Aspects of the experimental data on ejection dynamics can be interpreted based on mechanical models where frictional interactions with the capsid wall provide the resistive force that determines speed of translocation [16,17].

On the macroscale, the problem of inserting flexible fibers in cavities is encountered in medicine when catheters are inserted into body cavities during surgical or imaging procedures. For example, children and infants with hydrocephalus can be fitted with extended length peritoneal shunt catheters that drain into the abdominal cavity [18]. In coronary angioplasty, a thin catheter is guided through the confining walls of blood vessels following curved trajectories [19]. In such problems, it is important to understand the shape assumed by the fiber within the body cavity. This shape depends on the applied load, frictional interactions with the confining walls [20], and elastic properties of the fiber.

A related example is the buckling of drill string within a petroleum well. The drill string is confined in a cylindrical borehole, which in general has a curvilinear trajectory. Under the influence of compressive and torsional loading, and confined by the walls of the borehole, the drill string exhibits buckling instabilities. Sinusoidal, helical, and more complex structures can develop [21–24].

Analysis of the problem of the shape of a flexible fiber in a cavity sometimes assumes that the fiber remains in contact with the confining wall at all points. While this may be mostly true for a very long fiber under confinement, there may be “free-flying” sections at either end of the fiber. Here we consider an idealized model problem in order to study such end sections, which are completely absent in studies of the deformation of fibers or elastica which form a closed loop and therefore have no ends [25,26].

The geometry that we consider is shown in Fig. 1. We wish to determine the shape of the fiber as well as the force required to push the fiber into a container or capsid. Torsional loading is not considered, and friction between the fiber and the cylinder wall is neglected. The capsid is modeled as a smooth circular cylinder of radius  $a$ , with an entry hole at A and with inwards normal  $\hat{\mathbf{N}}$ . The fiber is sufficiently rigid that outside the capsid it is straight, with curvature  $\kappa = 0$ , and it is pushed into the capsid with a force  $F_1$ , which we seek to determine. Thus we assume that the unconstrained fiber outside the capsid is sufficiently short that Euler buckling does not occur. We use  $s$  as a coordinate along the length of the fiber, with  $s = s_1 < 0$  at the point of entry, and  $s = s_2$  at the end of the fiber, so that the length of the fiber within the capsid is  $L = s_2 - s_1 > 0$ . Within the capsid, the fiber is forced to curve around the inner surface of the cylinder and therefore has curvature  $\kappa = 1/a$  in

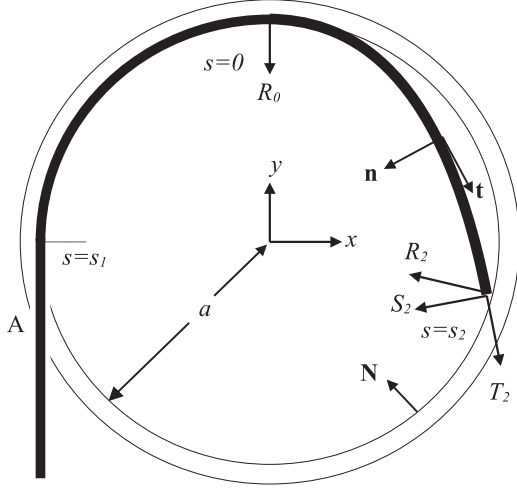


FIG. 1. The geometry considered in Secs. II and III. The fiber enters the cylinder at A, where the coordinate along the fiber is  $s = s_1 < 0$ . The portion  $s_1 < s < 0$  of the fiber is in contact with the inner surface of the cylinder, and the portion  $0 < s < s_2$  traverses the inside of the cylinder, which it contacts again at the fiber end  $s = s_2$ .

the region  $s_1 < s < 0$  where it is in continuous contact with the cylinder.

We assume that the fiber has Young's modulus  $E$  and cross-sectional area moment of inertia  $I$  about its midplane. The elastic energy of the fiber due to curvature is therefore

$$U(L) = \frac{EI}{2} \int_{s_1}^{s_2} \kappa^2 ds = -\frac{EIs_1}{2a^2} + \frac{EI}{2} \int_0^{s_2} \kappa^2 ds. \quad (1)$$

Once  $L$  is sufficiently large, any further increase in the length of fiber inside the cylinder leaves the free-flying section (of length  $s_2$ ) unchanged and merely changes the length  $-s_1$  of the portion of the fiber in continuous contact with the cylinder wall. The work required to push a further length  $\delta L = -\delta s_1$  of the fiber into the capsid is therefore  $F_1 \delta L$ , and the increase in elastic potential energy is  $EI \delta L / (2a^2)$ . This suggests that force required to push the fiber into the capsid is

$$F_1 = \frac{EI}{2a^2}. \quad (2)$$

The analysis tells us nothing about the stresses within the fiber, nor the forces acting at the couple-free end of the fiber at  $s = s_2$ . In the next section, we examine the force balance in more detail. The analysis combines recent work on tangential forces due to a smooth confining sleeve [27–31] with an analysis of free-flying sections of an elastica [32].

## II. THE BEAM EQUATIONS

The state of stress within the fiber may be studied using the classical beam equations [33]. We use  $s$  as a coordinate along the length of the fiber, which has unit tangent  $\hat{\mathbf{t}}$ , unit normal  $\hat{\mathbf{n}}$ , and binormal  $\hat{\mathbf{b}}$ . The state of stress within the fiber at  $s = \sigma$  may be characterized by the force  $\mathbf{F}(\sigma)$  due to the portion of the fiber in  $s > \sigma$  acting on the portion in  $s < \sigma$ , together with

the moment  $\mathbf{M}(\sigma)$  of the force in  $s > \sigma$  acting on the fiber in  $s < \sigma$ . Equilibrium of moments and forces requires

$$\frac{d\mathbf{M}}{ds} + \hat{\mathbf{t}} \times \mathbf{F} = -\mathbf{\Gamma}_e, \quad (3a)$$

$$\frac{d\mathbf{F}}{ds} = -\mathbf{\Phi}_e, \quad (3b)$$

where  $\mathbf{\Gamma}_e$  and  $\mathbf{\Phi}_e$  are the external moment and force per unit length acting on the fiber. In the problem considered here the only external couple acting on the fiber is that caused by the constraint of the hole in the capsid wall through which the fiber passes; the only external forces are the force  $F_1$  pushing the fiber into the container and the reaction due to contact with the smooth wall, which is everywhere in the direction of the local normal to the wall,  $\hat{\mathbf{N}}$ , except at the entry hole where the constraint applies a tangential force (despite the assumption that the hole through which the fiber passes is smooth). This tangential force is sometimes described as an Eshelby-like force, found by variational analysis of the potential energy of the fiber together with the material momentum balance law [27,29]. A more physical explanation, due to Balabukh *et al.* [31], is given by Bigoni *et al.* [28]. We therefore assume

$$\mathbf{\Phi}_e = R\hat{\mathbf{N}} + G\hat{\mathbf{t}}, \quad (4)$$

where the tangential force is zero (due to the zero friction) everywhere except at the exit to the constraining hole inside the capsid, where the curvature of the fiber changes from 0 to  $a^{-1}$ . Experiments in which the effects of this tangential force is observed are discussed in [27,28], and there is further theoretical discussion in [29,30].

The normal  $\hat{\mathbf{n}}$  to the curved fiber is aligned with  $\hat{\mathbf{N}}$  wherever the fiber is in continuous contact with the cylinder wall. Equation (3a) is supplemented by the constitutive relation

$$\mathbf{M} = EI\kappa\hat{\mathbf{b}}, \quad (5)$$

and we resolve  $\mathbf{F}$  as

$$\mathbf{F} = T\hat{\mathbf{t}} + S\hat{\mathbf{n}}, \quad (6)$$

so that

$$\hat{\mathbf{t}} \times \mathbf{F} = S\hat{\mathbf{b}}. \quad (7)$$

We assume (for now) that the fiber is constrained to enter the capsid tangentially. The moment balance (3a) becomes

$$EI \frac{d\kappa}{ds} + S = EI\kappa_1 \delta(s - s_1), \quad (8)$$

where we assume that a point couple

$$\mathbf{\Gamma}_e = -EI\kappa_1 \delta(s - s_1) \hat{\mathbf{b}}, \quad (9)$$

imposed at the entry hole  $s = s_1$ , is responsible for a jump change in curvature from  $\kappa = 0$  outside the capsid to  $\kappa = \kappa_1$  inside. Thus  $\kappa = \kappa_1 H(s - s_1)$  in the neighborhood of  $s_1$ , where  $H$  is the Heaviside function. Our assumption that the fiber immediately comes into contact with the wall implies  $\kappa_1 = a^{-1}$ , but we shall later consider entry conditions with  $\kappa_1 \neq a^{-1}$ . With the orientation of  $\hat{\mathbf{t}}$  and  $\hat{\mathbf{n}}$  indicated in Fig. 1, the binormal  $\hat{\mathbf{b}}$  is directed into the page, and the negative couple represented by the right-hand side of (8) is a couple in the anticlockwise direction.

The tangential force (4) at the exit from a straight sleeve is [27–29]

$$G = \frac{EI}{2} \kappa_1^2 \delta(s - s_1). \quad (10)$$

The Frenet-Serret equations for a plane curve

$$\frac{d\hat{\mathbf{t}}}{ds} = \kappa \hat{\mathbf{n}}, \quad \frac{d\hat{\mathbf{n}}}{ds} = -\kappa \hat{\mathbf{t}}, \quad (11)$$

imply that

$$\frac{d\mathbf{F}}{ds} = \left( \frac{dT}{ds} - \kappa S \right) \hat{\mathbf{t}} + \left( \frac{dS}{ds} + \kappa T \right) \hat{\mathbf{n}}. \quad (12)$$

Hence Eq. (3b) can be resolved as

$$\frac{dT}{ds} - \kappa S = -\frac{EI}{2} \kappa_1^2 \delta(s - s_1), \quad (13)$$

$$\frac{dS}{ds} + \kappa T = -R, \quad (14)$$

where the normal reaction  $R \geq 0$ . We use (8) to eliminate  $S$  from (13) and obtain

$$\frac{dT}{ds} + \kappa EI \frac{d\kappa}{ds} - \kappa EI \kappa_1 \delta(s - s_1) = -\frac{EI}{2} \kappa_1^2 \delta(s - s_1). \quad (15)$$

Noting that  $\int H(s) \delta(s) ds = 1/2$  if the range of integration includes the origin, we integrate (15) to obtain

$$T + \frac{EI}{2} \kappa^2 = -C = \frac{EI}{a^2} C_2, \quad (16)$$

where  $C = -C_2 EI/a^2$  is a constant of integration, equivalent (in the absence of gravity) to the material force  $\mathcal{C}$  used, e.g., by O'Reilly [29].

In  $s < s_1$  the fiber curvature  $\kappa = 0$  and the fiber is in compression, so  $T = -F_1$  and  $C = F_1 > 0$ .

### III. THE UNSUPPORTED ELASTICA

We now examine the region  $s > 0$  in which the fiber is no longer in contact with the inner surface of the capsid cylinder (Fig. 1). We assume that the end of the fiber contacts the cylinder at  $s = s_2$  (as yet unknown). This final section  $0 < s < s_2$  of the fiber takes the form of an unsupported elastica, similar to those studied in [32,34–37].

We set up Cartesian coordinates  $(x, y)$  with origin at the center of the circle and with  $x$  tangential to the cylinder wall (and fiber) at  $s = 0$ , so that  $s = 0$  corresponds to the point with Cartesian coordinates  $(0, a)$ , as shown in Fig. 1. We describe the orientation of the tangent to the fiber by an angle  $\theta$ , with  $\theta = 0$  along the  $x$  axis. We nondimensionalize all lengths by  $a$ , forces by  $EI/a^2$ , and moments by  $EI/a$ . The shear force  $S = 0$  in  $s_1 < s < 0$ , since  $\kappa = 1$  is constant. We assume that there is a point force reaction at  $s = 0$ , and write this nondimensionalized reaction in the form  $R = R_0 \delta(s)$ . This reaction is normal to the friction-free surface of the confining cylinder, which is smooth except at the corner of the inlet hole.

We consider the various forces acting on the fiber in  $s > s_1$ . All reaction forces are normal to the cylinder and have zero moment about the axis of the cylinder. At  $s_1$  the couple  $\Gamma_e$  (9) acts on the fiber, as does the force  $-T(s_1^+) = -C_2 + \frac{1}{2}$ , where we use the superscript  $+$  to denote a limit as  $s$  approaches  $s_1$

from above. The (nondimensional) balance of couples about the axis therefore requires

$$C_2 = -\frac{1}{2}. \quad (17)$$

We conclude from (16) that in  $s < s_1$ , outside the capsid, where the curvature of the fiber is assumed to be zero,

$$T = -F_1 = -\frac{1}{2} \quad (18)$$

[or, in dimensional form,  $F_1 = EI/(2a^2)$ ] in agreement with the result (2) obtained by virtual work arguments.

Integrating (14) across  $s = 0$ , we find that the shear force at  $s = 0^+$  is

$$S(0^+) = -R_0. \quad (19)$$

We now eliminate  $T$  and  $S$  from (14), using (8) and (16), to obtain

$$\frac{d^2 \kappa}{ds^2} + \frac{\kappa^3}{2} - C_2 \kappa = 0. \quad (20)$$

This can be integrated once to give

$$\frac{1}{2} \left( \frac{d\kappa}{ds} \right)^2 + \frac{\kappa^4}{8} - C_2 \frac{\kappa^2}{2} = D, \quad (21)$$

where  $D$  is a constant of integration that can be evaluated in terms of  $C_2$  and the values  $\kappa = 1$  and [by (8) and (19)]  $d\kappa/ds = R_0$  at  $s = 0^+$ . The shape of an elastica can be expressed in terms of elliptic integrals (see, e.g., [26,32]), but it is more convenient here to integrate (20) numerically to obtain  $\kappa(s)$ . If the tangent to the fiber is at angle  $\theta$  to the  $x$  axis, then

$$\frac{d\theta}{ds} = -\kappa, \quad (22)$$

and we note that  $\theta < 0$  for suitably small values of  $s > 0$ . As we move along the fiber from  $s = 0$ , the Cartesian coordinates evolve as

$$\frac{dx}{ds} = \cos \theta, \quad \frac{dy}{ds} = \sin \theta. \quad (23)$$

The nondimensional governing equation (20) can be rewritten in a form suitable for numerical integration:

$$\frac{d\kappa}{ds} = \lambda, \quad \frac{d\lambda}{ds} = C_2 \kappa - \frac{\kappa^3}{2}, \quad \frac{d\theta}{ds} = -\kappa, \quad (24a)$$

$$\frac{dx}{ds} = \cos \theta, \quad \frac{dy}{ds} = \sin \theta, \quad (24b)$$

with initial conditions

$$\begin{aligned} \kappa &= 1, & \frac{d\kappa}{ds} &= \lambda = R_0, & \theta &= 0, & x &= 0, \\ y &= 1, & \text{at } s &= 0. \end{aligned} \quad (25)$$

The point force reaction  $R_0$  is unknown and must be determined so as to ensure that boundary conditions (discussed below) are satisfied at the end of the fiber. We integrate these equations (24) numerically, using the MATLAB routine ode45, until the fiber hits the cylinder again, which occurs at  $s = s_2$  (determined as part of the solution), where  $\kappa = \kappa_2$ ,  $\theta = \theta_2$ , and  $(x, y) = (x_2, y_2)$  with  $x_2^2 + y_2^2 = 1$ . The outward normal at the point of contact is at an angle  $\phi_2 = \tan^{-1}(y_2/x_2)$

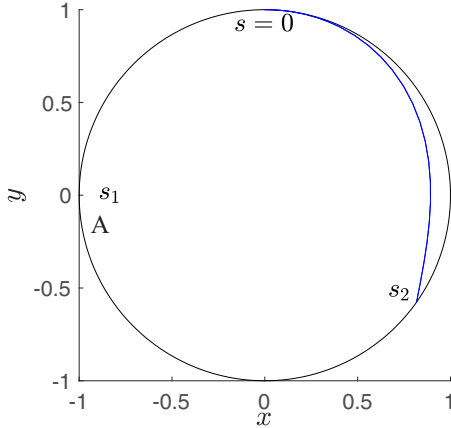


FIG. 2. The trajectory satisfying the boundary condition (28), corresponding to a point force reaction  $R_0 = 0.7053$  with  $C_2 = -0.5$ . The fiber enters the cylinder at A, where  $s = s_1$ , and remains in contact with the cylinder wall up to  $s = 0$ .

to the  $x$  axis. The components of the force on the end of the fiber are

$$T_2 = C_2 - \kappa_2^2/2, \quad S_2 = -\frac{d\kappa}{ds}. \quad (26)$$

The total force acting on the end of the fiber at  $s = s_2$  has components

$$F_{2x} = T_2 \cos \theta_2 + S_2 \sin \theta_2, \quad (27a)$$

$$F_{2y} = T_2 \sin \theta_2 - S_2 \cos \theta_2, \quad (27b)$$

and we require that these are the components of the normal force at the wall, which is along the direction  $(n_x, n_y) = (-x, -y)$ . Hence we require

$$\frac{n_x}{n_y} = \frac{x_2}{y_2} = \frac{F_{2x}}{F_{2y}}. \quad (28)$$

The choice  $R_0 = 0.7053$  gives the solution satisfying the boundary condition (28) shown in Fig. 2 with the end of the fiber at  $s_2 = 2.0888$ : these values agree with those found by Romero *et al.* [32]. At the end of the fiber,  $(x_2, y_2) = (0.8172, -0.5764)$ , the curvature  $\kappa_2 = 0$ , the tangent to the fiber is at an angle  $\theta_2 = -1.7641$  rad to the  $x$  axis, the shear force  $S_2 = 1.1168$ , and the tension  $T_2 = -0.5$ . As a result,  $F_{2x} = -1$  and  $F_{2y} = 0.7053$ , so the forces on the fiber at  $s_2$  are equal and opposite to those acting on it at  $s = 0$ . The tangent to the fiber at its point of contact with the wall is at an angle  $\psi_2 = 1.15$  rad to the normal to the cylinder.

The length of fiber within the cylinder,  $s_2 - s_1$ , has been assumed greater than  $s_2$ , but is otherwise unconstrained. Our assumption that the fiber lies within a cross-sectional plane of the cylinder means that if  $|s_1| > 2\pi$  the fiber overlaps itself as it wraps around the inside of the cylinder. In practice, the fiber might take the form of a closely wound helix, such as those seen in experiments [5,12], particularly when friction is low [13].

#### IV. OTHER ENTRANCE CONDITIONS

##### A. A fiber freely orientated at the entry point

We have so far assumed that the fiber passes through a cylindrical hole in the capsid wall that forces the fiber to enter tangentially and immediately conform to the curvature of the confining wall. One could alternatively imagine the fiber to pass through a hole in a thin-walled cylinder. The hole fixes the position of the fiber as it enters and may impose a force on the fiber, but it does not constrain the orientation of the fiber, nor can it impose a couple. The fiber does not immediately come into contact with the cylinder wall, so there is a section of free-flying fiber inside the cylinder immediately after the entrance hole. In the absence of any imposed couple at the entry hole, the balance of couples acting on the fiber about the axis of the cylinder now requires that the force on the fiber at the entrance hole is normal to the cylinder wall. The free-flying section at the entrance is therefore a suitably orientated mirror image of the free-flying section  $s > 0$  at the end of the fiber. The force required to push the fiber into the hole is  $T = -0.5$ , again in agreement with the result (2) of the simple energy analysis. Examples of computed shapes will be given in Sec. V, where they will be compared against experiment.

##### B. A fiber with prescribed orientation at the entry point

In Secs. II and III we assumed that the fiber was constrained to enter the cylinder tangentially, but other constrained orientations of the fiber are possible at the entrance. We now consider the case in which the fiber is constrained to pass perpendicular to the wall of the cylinder. The fiber then crosses the interior of the cylinder before landing on the opposite wall. The unsupported elastica is governed by the same equations as before, and the constant  $C_2 = -0.5$ , as before, in order to maintain the balance of forces and couples acting on the free-flying end section of the fiber. The computation of the fiber shape at the entrance, shown in Fig. 3, was started at  $(x, y) = (0, 1)$ , which was taken to be the origin  $s = 0$ . The reaction force  $R_0$  at  $s = 0$  was used as a shooting parameter: the computation was continued along the fiber to the opposite wall, which the fiber intersected perpendicularly at  $s = s_1 = -2.697$  when the reaction force was chosen to be  $R_0 = 1.848$ . This entry point  $s_1$  is at  $(x, y) = (x_1, y_1) = (0.255, -0.967)$ , where the curvature (just inside the cylinder) is  $\kappa_1 = -1.437$  and the shear stress (8) is  $S_1 = -d\kappa/ds = 1.437$ . The computed forces and couples at the two ends of the unsupported elastica are in equilibrium to within 0.2%. The tension in the fiber just inside the cylinder, at  $s = s_1^+$  is, by (16),  $T_1 = C_2 - \kappa_1^2/2 = -1.5328$ , but the tension outside is again  $T_1 = C_2 = -0.5$ .

Figure 3 shows the trajectory of a fiber constrained to enter the cylinder perpendicular to the cylinder wall at  $(x, y) = (0.255, -0.967)$ . The incoming fiber, of length  $-s_1 = 2.697$  occupies the left-hand portion of the figure and contacts the cylinder at  $(x, y) = (0, 1)$ , after which the final fiber section of length  $s_2 = 2.0888$  is shown. If the fiber has total length greater than  $s_2 - s_1$ , the additional length would touch the cylinder wall along a circular arc between the two free-flying sections.

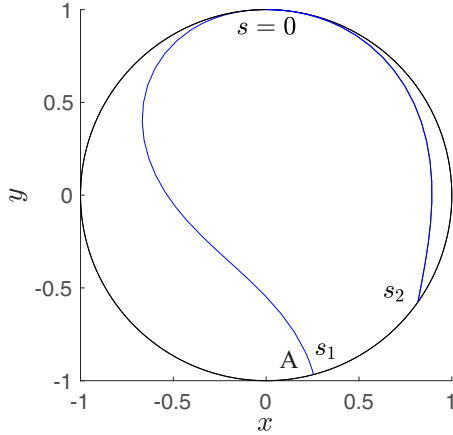


FIG. 3. The trajectory of a fiber constrained to enter the cylinder perpendicular to the cylinder wall at A, where  $(x, y) = (0.255, -0.967)$  and  $s = s_1 = -2.697$ . The incoming fiber contacts the cylinder at  $s = 0$ , where  $(x, y) = (0, 1)$ , after which the final fiber section of length  $s_2 = 2.0888$  is shown. If the fiber has total length greater than  $s_2 - s_1$ , the additional length would touch the cylinder wall along a circular arc between the two free-flying sections, rather than at the single point  $s = 0$ .

More generally, any angle  $\psi_1$  can be imposed between the tangent to the fiber at its point of entry and the normal to the cylinder wall at this point.  $\psi_1 = 0$  corresponds to perpendicular entry, discussed above, whereas  $\psi_1 = \pi/2$  corresponds to tangential entry, discussed in Secs. II and III. We consider an elastica that enters the cylinder at  $s = s_1 < 0$  and regains contact with the cylinder wall at  $s = 0$ ; Fig. 4 shows  $s_1(\psi_1)$ . We note that multiple solutions are sometimes possible, though highly tortuous shapes require a higher bending energy and are not discussed here. Solutions for  $-\pi/2 < \psi_1 < 0$  are the mirror image (about the plane of symmetry through the point

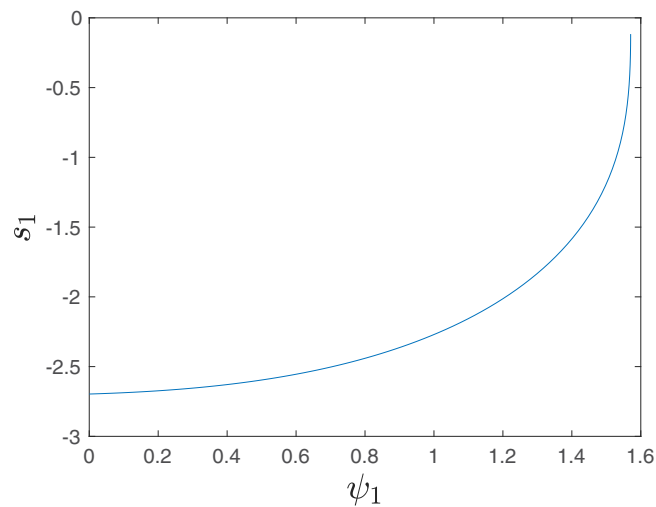


FIG. 4. Plot of  $s_1$  at the entrance against the imposed entry angle  $\psi_1$  (radians) for an unsupported elastica regaining contact with the cylinder wall at  $s = 0$ . The length of the unsupported section of elastica is  $-s_1$ . The elastica shown entering the cylinder at A in Fig. 3 corresponds to  $\psi_1 = 0$ , whereas tangential entry ( $\psi_1 = \pi/2$ ) contacts the wall immediately.



FIG. 5. A steel hacksaw blade of length  $L_H = 266 \text{ mm} = 4.97a$  confined within a PVC pipe coupling of diameter  $2a = 107 \text{ mm}$ . The dashed line is the fiber shape predicted in Secs. III and IV A.

of entry) of solutions for  $-\psi_1 > 0$ . Sufficiently high forces can lead a free-flying section of the elastica to contact itself, as seen in the computations of Alben [38] and, in a somewhat different geometry, those of Lu and Chen [39].

V. EXPERIMENTS

Experiments to verify the shape of the free-flying section were performed with steel hacksaw blades confined within a circular 4 inch PVC pipe coupling of internal diameter  $2a = 107 \text{ mm}$ . Figure 5 shows a blade, of length  $L_H = 266 \text{ mm} = 4.97a$ , within the pipe. The experiments are similar to those of Romero *et al.* [32] in which paper or mica sheets were coiled within a cylinder, but differ somewhat from those of De Tommasi *et al.* [26] who studied deformation of an elastic ring (which had no ends) confined within a cylinder.

There is no entry hole in the experiments, and the configuration of the blade should be symmetric about its midpoint. Both ends of the fiber are constrained solely by a reaction force normal to the curved wall of the cylinder, and the orientation of neither end is constrained by the wall. This is the scenario discussed in Sec. IV A for the shape of the fiber within the cylinder when the entry hole does not constrain the fiber orientation. Also shown in Fig. 5, as a red dashed line, is the computed fiber shape. This consists of the two free-flying end sections, each of nondimensional length  $s_2$ , together with a central circular arc of nondimensional length  $L_H a^{-1} - 2s_2$ . Agreement between experiment and theory is good.

Figure 6 shows a second experiment with the same PVC pipe but a longer hacksaw blade of length  $L_H = 315 \text{ mm} = 5.89a$ . In this second experiment friction between the blade and the pipe walls was higher, allowing multiple equilibrium



FIG. 6. As for Fig. 5, but with a hacksaw blade of length  $L_H = 315 \text{ mm} = 5.89a$ . The dashed line is the fiber shape predicted in Secs. III and IV A.

configurations. The inside of the pipe was coated with grease in an attempt to reduce the friction.

The longer blade showed significant plastic deformation after removal from the PVC pipe section. The shorter blade showed some plastic deformation but less than that of the longer blade. This difference may be due to the greater deformation to which the longer blade was subjected, but may also be due to differences in the composition of the steel.

## VI. CONCLUDING REMARKS

A problem in microbiology that has been studied experimentally using modern methods of single-molecule manipulation is DNA packing and ejection from bacteriophages. Double-stranded DNA (dsDNA) can be modeled as a highly charged semiflexible elastic rod subject to fluctuating Brownian forces. The persistence length  $l_p = EI/(kT)$  (where  $kT$  is the Boltzmann temperature) of dsDNA is typically of the order of 25–50 nm [40]. Since this is of the same order as the diameter of the protein capsids in which the phage DNA is packaged, the equilibria and dynamics of elastica in confined cavities provide an appropriate paradigm for describing the interactions between DNA and capsid. Taking  $l_p = a = 50 \text{ nm}$  and  $T = 300 \text{ K}$ , we find a force  $F_1 = EI/(2a^2) \approx 40 \text{ fN}$ . In practice, once the capsid starts to fill, the curvature of the packed DNA inevitably increases [41], and as spacings between segments become smaller, other effects (e.g., electrostatic repulsions) start to play a role. As a result Smith *et al.* [42] measured a force that increased eventually to 55 pN. Experimentally measured forces are discussed in more detail by Purohit *et al.* [3].

Two classes of problems have been studied previously: the insertion of DNA into capsids during synthesis of the virus and ejection of DNA from the capsid when the phage infects a bacterial cell by attaching itself to the cell membrane and injecting its DNA into the cytosol. In the first case,

molecular motors do work against the electrostatic self-energy and elastic bending energy of the DNA molecule. The slowing of the molecular motor as more of the DNA is packaged can be measured [42]. In the second case, the DNA is forcibly ejected due to the release of elastic and electrostatic self-energy of the confined DNA and the slowing of the DNA ejection velocity as the capsid empties can be quantified experimentally [43]. Typically, the electrostatic self-energy and the elastic bending energy contribute about equally to the potential energy of the confined DNA, though the electrostatic part can be eliminated in controlled experiments by the addition of multivalent ions [44]. The equilibrium [3,7] as well as the nonequilibrium [16,17] (with friction) problems have been studied using the constrained elastica paradigm. However, since the total DNA length ( $\approx 17 \mu\text{m}$  for the lambda phage) is typically very large compared to the capsid diameter  $\approx 50 \text{ nm}$ , any free-flying sections at the ends of the DNA generally do not play an important role in the energetics, except during relatively short time intervals at the beginning and end of the ejection process. Indeed, in most theoretical models, one regards the DNA as spooled in contact with the capsid wall with a radius of curvature that progressively decreases as more of the space within the capsid becomes filled. Nevertheless, the existence of free-flying sections is confirmed in Brownian dynamics simulations using a “chain of beads” model for the DNA [7]. These simulations show that once the packing fraction of the capsid becomes sufficiently high, the inner region of the DNA stops spooling in ever tighter circles and makes loose coils parallel to the spool axis near the end of the DNA. When DNA packs into phages, the DNA enters the capsid through a long narrow tubular structure called the “tail.” This is also the structure that attaches to the host cell and through which the DNA passes during ejection. Thus, the fiber enters the capsid in a direction perpendicular to the wall resulting in free-flying sections at both the entrance to the capsid and at the end of the fiber.

Friction between the fiber and cylinder wall has been ignored in the computations presented here. Friction will not only modify the computed elastica shapes, but also introduce new effects, such as the possibility of rolling contact, rather than sliding contact, and hysteresis, as discussed in [20,37].

We have not discussed the behavior of the fiber outside the cylinder. If we regard the straight section of fiber outside the cylinder as an Euler buckling beam with fixed ends, the applied force  $EI/(2a^2)$  would cause buckling once the length of the straight section exceeds  $2^{3/2}\pi a$ .

## ACKNOWLEDGMENTS

J.D.S. thanks the Department of Applied Mathematics and Theoretical Physics, University of Cambridge, for virtual hospitality. We thank an anonymous reviewer for drawing our attention to relevant references, particularly [27–31] concerning tangential forces due to confinement by a smooth tube.

[1] C. M. Knobler and W. M. Gelbart, Physical chemistry of DNA viruses, *Annu. Rev. Phys. Chem.* **60**, 367 (2009).

[2] M. De Frutos, A. Leforestier, and F. Livolant, Relationship between the genome packing in the bacteriophage capsid and the kinetics of DNA ejection, *Biophys. Rev. Lett.* **9**, 81 (2014).

- [3] P. K. Purohit, M. M. Inamdar, P. D. Grayson, T. M. Squires, J. Kondev, and R. Phillips, Forces during bacteriophage DNA packaging and ejection, *Biophys. J.* **88**, 851 (2005).
- [4] K. E. Richards, R. C. Williams, and R. Calendar, Mode of DNA packing within bacteriophage heads, *J. Mol. Biol.* **78**, 255 (1973).
- [5] W. C. Earnshaw and S. C. Harrison, DNA arrangement in isometric phage heads, *Nature (London)* **268**, 598 (1977).
- [6] M. E. Cerritelli, N. Cheng, A. H. Rosenberg, C. E. McPherson, F. P. Booy, and A. C. Steven, Encapsidated conformation of bacteriophage T7 DNA, *Cell* **91**, 271 (1997).
- [7] J. Kindt, S. Tzlil, A. Ben-Shau, and W. M. Gelbart, DNA packaging and ejection forces in bacteriophage, *Proc. Natl. Acad. Sci. USA* **98**, 13671 (2001).
- [8] M. A. F. Gomes, V. P. Brito, and M. S. Araújo, Geometric properties of crumpled wires and the condensed non-solid packing state of very long molecular chains, *J. Braz. Chem. Soc.* **19**, 293 (2008).
- [9] N. Stoop, J. Najafi, F. K. Wittel, M. Habibi, and H. J. Herrmann, Packing of Elastic Wires in Spherical Cavities, *Phys. Rev. Lett.* **106**, 214102 (2011).
- [10] R. Vetter, F. K. Wittel, N. Stoop, and H. J. Herrmann, Finite element simulation of dense wire packings, *Eur. J. Mech. A Solids* **37**, 160 (2013).
- [11] T. A. Sobral, M. A. F. Gomes, N. R. Machado, and V. P. Brito, Unpacking of a crumpled wire from two-dimensional cavities, *PLoS ONE* **10**, e0128568 (2015).
- [12] V. H. de Holanda and M. A. F. Gomes, Scaling, crumpled wires, and genome packing in virions, *Phys. Rev. E* **94**, 062406 (2016).
- [13] M. R. Shaebani, J. Najafi, A. Farnudi, D. Bonn, and M. Habibi, Compaction of quasi-one-dimensional elastoplastic materials, *Nat. Commun.* **8**, 15568 (2017).
- [14] T. Curk, J. D. Farrell, J. Dobnikar, and R. Podgornik, Spontaneous Domain Formation in Spherically Confined Elastic Filaments, *Phys. Rev. Lett.* **123**, 047801 (2019).
- [15] M. Piñeira, M. Adda-Bedia, and S. Moulinet, Spooling and disordered packing of elastic rods in cylindrical cavities, *Europhys. Lett.* **104**, 14005 (2013).
- [16] S. Ghosal, Capstan Friction Model for DNA Ejection from Bacteriophages, *Phys. Rev. Lett.* **109**, 248105 (2012).
- [17] R. Arun and S. Ghosal, A mechanical model of bacteriophage DNA ejection, *Phys. Lett. A* **381**, 2386 (2017).
- [18] W. T. Couldwell, D. R. Lemay, and J. G. McComb, Experience with use of extended length peritoneal shunt catheters, *J. Neurosurgery* **85**, 425 (1996).
- [19] P. A. Schneider, *Endovascular Skills: Guidewire and Catheter Skills for Endovascular Surgery* (Marcel Dekker, New York, 2003).
- [20] C.-W. Liu and J.-S. Chen, Effect of Coulomb friction on the deformation of an elastica constrained in a straight channel with clearance, *Eur. J. Mech. A Solids* **39**, 50 (2013).
- [21] J. M. T. Thompson, M. Silveira, G. H. M. van der Heijden, and M. Wiercigroch, Helical post-buckling of a rod in a cylinder: With applications to drill-strings, *Proc. R. Soc. A* **468**, 1591 (2012).
- [22] C. Sun and S. Lukasiewicz, A new model on the buckling of a rod in tubing, *J. Petrol. Sci. Eng.* **50**, 78 (2006).
- [23] G. H. M. van der Heijden, A. R. Champneys, and J. M. T. Thompson, Spatially complex localisation in twisted elastic rods constrained to a cylinder, *Int. J. Solids Struct.* **39**, 1863 (2002).
- [24] J.-P. Liu, X.-Y. Zhong, Z.-B. Cheng, X.-Q. Feng, and G.-X. Ren, Buckling of a slender rod confined in a circular tube: Theory, simulation, and experiment, *Int. J. Mech. Sci.* **140**, 288 (2018).
- [25] P. Vázquez-Montejo, Z. McDargh, M. Deserno, and J. Guven, Cylindrical confinement of semiflexible polymers, *Phys. Rev. E* **91**, 063203 (2015).
- [26] D. De Tommasi, G. Devillanova, F. Maddalena, G. Napoli, and G. Puglisi, Elastic multi-blisters induced by geometric constraints, *Proc. R. Soc. A* **477**, 20200562 (2021).
- [27] F. Bosi, D. Misseroni, F. Dal Corso, and D. Bigoni, An elastica arm scale, *Proc. R. Soc. A* **470**, 20140232 (2014).
- [28] D. Bigoni, F. Dal Corso, F. Bosi, and D. Misseroni, Eshelby-like forces acting on elastic structures: Theoretical and experimental proof, *Mech. Mater.* **80**, 368 (2015).
- [29] O. M. O'Reilly, Some perspectives on Eshelby-like forces in the elastica arm scale, *Proc. R. Soc. A* **471**, 20140785 (2015).
- [30] J. A. Hanna, H. Singh, and E. G. Virga, Partial constraint singularities in elastic rods, *J. Elast.* **133**, 105 (2018).
- [31] L. I. Balabukh, M. N. Vulfson, B. V. Mukoseev, and Ya. G. Panovko, On work done by reaction forces of moving supports, *Research on Theory of Constructions* (Moscow, 1970), Vol. 18, pp. 190–200.
- [32] V. Romero, T. A. Witten, and E. Cerda, Multiple coiling of an elastic sheet in a tube, *Proc. R. Soc. A* **464**, 2847 (2008).
- [33] L. D. Landau and E. M. Lifshitz, *Theory of Elasticity*, 2nd ed. (Pergamon, Oxford, 1970).
- [34] R. C. Benson, The deformation of a thin, incomplete, elastic ring in a frictional channel, *J. Appl. Mech.* **48**, 895 (1981).
- [35] G. M. Griner, A parametric solution to the elastic pole-vaulting pole problem, *J. Appl. Mech.* **51**, 409 (1984).
- [36] J. Stolte and R. C. Benson, An extending dynamic elastica: Impact with a surface, *J. Vib. Acoust.* **115**, 308 (1993).
- [37] T. G. Sano, T. Yamaguchi, and H. Wada, Slip Morphology of Elastic Strips on Frictional Rigid Substrates, *Phys. Rev. Lett.* **118**, 178001 (2017).
- [38] S. Alben, Packing of elastic rings with friction, *Proc. R. Soc. A* **478**, 20210742 (2022).
- [39] Z.-H. Lu and J.-S. Chen, Deformations of a clamped–clamped elastica inside a circular channel with clearance, *Int. J. Solids Struct.* **45**, 2470 (2008).
- [40] G. S. Manning, The persistence length of DNA is reached from the persistence length of its null isomer through an internal electrostatic stretching force, *Biophys. J.* **91**, 3607 (2006).
- [41] P. K. Purohit, J. Kondev, and R. Phillips, Mechanics of DNA packaging in viruses, *Proc. Natl. Acad. Sci. USA* **100**, 3173 (2003).
- [42] D. E. Smith, S. J. Tans, S. B. Smith, S. Grimes, D. L. Anderson, and C. Bustamante, The bacteriophage straight  $\phi$ 29 portal motor can package DNA against a large internal force, *Nature (London)* **413**, 748 (2001).
- [43] P. Grayson, L. Han, T. Winther, and R. Phillips, Real-time observations of single bacteriophage  $\lambda$  DNA ejections in vitro, *Proc. Natl. Acad. Sci. USA* **104**, 14652 (2007).
- [44] A. Evilevitch, M. Castelnovo, C. M. Knobler, and W. M. Gelbart, Measuring the force ejecting DNA from phage, *J. Phys. Chem. B* **108**, 6838 (2004).